CdS nanofilms: Effect of film thickness on morphology and optical band gap

Suresh Kumar, Santosh Kumar, Pankaj Sharma, Vineet Sharma, and S. C. Katyal

Citation: J. Appl. Phys. **112**, 123512 (2012); doi: 10.1063/1.4769799
View online: http://dx.doi.org/10.1063/1.4769799
View Table of Contents: http://jap.aip.org/resource/1/JAPIAU/v112/i12
Published by the American Institute of Physics.

CdS nanofilms: Effect of film thickness on morphology and optical band gap

Suresh Kumar,[1] Santosh Kumar,[2] Pankaj Sharma,[1,a)] Vineet Sharma,[1] and S. C. Katyal[3]
[1]*Department of Physics, Jaypee University of Information Technology, Waknaghat, Solan-173234, Himachal Pradesh, India*
[2]*Applied Chemistry Department, Faculty of Technology and Engineering, The M. S. University of Baroda, Vadodara 390001, Gujarat, India*
[3]*Department of Physics, Jaypee Institute of Information Technology, Sec-128, Noida 201301, Uttar Pradesh, India*

(Received 24 September 2012; accepted 16 November 2012; published online 19 December 2012)

CdS nanofilms of varying thickness (t) deposited by chemical bath deposition technique have been studied for structural changes using x-ray diffractometer (XRD) and transmission electron microscope (TEM). XRD analysis shows polycrystalline nature in deposited films with preferred orientation along (*002*) reflection plane also confirmed by selected area diffraction pattern of TEM. Uniform and smooth surface morphology observed using field emission scanning electron microscope. The surface topography has been studied using atomic force microscope. The optical constants have been calculated from the analysis of $\%T$ and $\%R$ spectra in the wavelength range 300 nm-900 nm. CdS nanofilms show a direct transition with red shift. The optical band gap decreases while the refractive index increases with increase in thickness of nanofilms. © *2012 American Institute of Physics*. [http://dx.doi.org/10.1063/1.4769799]

I. INTRODUCTION

CdS, in the form of films, has shown potential in variety of applications including visible radiation detection, window layers for photovoltaic solar cells, light emitting diodes (LEDs), gas sensors, piezoelectric devices, non-linear integrated optical devices, photocatalysts, etc.[1–7] The efficiency of optoelectronic devices can be improved by reducing the front (window) layer absorbance and hence the thickness so that most of solar radiations are transmitted quite freely.[2] In heterojunction solar cell, it is well known that higher short circuit current can be achieved by reducing thickness of window layer to improve blue spectral response.[2] Chemical bath deposition (CBD) is an inexpensive method and has become popular to deposit nanostructured thin films due to its various advantages, such as simplicity, low temperature, choice of substrates, large area coating, etc.[8–12] In addition, CBD offered vertical growth of crystallites in columnar form with c-axis perpendicular to the substrate.[12] This provides less grain boundaries parallel to the junction for controlling the flow of the excess carriers to the collector electrode. The film thickness plays an important role in the properties and the performance of devices based on CdS films. However, in literature the effect of film thickness on morphological and optical band gap of nanostructured CdS films is scantly reported.[13,14]] Therefore, the present communication reports the effect of film thickness on the structural, morphological, and optical properties of CdS nanofilms deposited via CBD technique.

II. EXPERIMENTAL DETAILS

CdS nanofilms have been deposited on glass substrate using the reagents $CdCl_2H_2O$: 0.02 M, $CS(NH_2)_2$: 0.04 M, NH_4OH: 2 M and triton (TX-100: 5%). All the reagents of AR-grade (Merck) and used without further purification. The details of the experimental procedure have been given elsewhere.[11] All the depositions have been carried out in alkaline medium prepared by double distilled water (Millipore, 15 MΩ-cm) at $p\mathrm{H} = 11 \pm 0.1$ and bath temperature $70 \pm 2\,^{\circ}\mathrm{C}$. The film thickness has been controlled by varying deposition time and successive depositions. After deposition, films have been ultrasonicated with 20% methanol solution to remove loosely adherent CdS particles. As deposited films are pale yellow to light orange in color, uniform and show good adhesion with the substrate. After deposition all films have been annealed at 573 ± 5 K.

A. Characterization

The film thickness has been measured by a stylus profilometer (AMBIOS XP-1, USA) after forming a step between film and substrate. X-ray diffractometer (XRD; PANalytical's X'Pert PRO) with CuKα radiation ($\lambda = 1.5406$ Å) in grazing angle mode has been used to study the crystal structure of the films. Transmission electron microscope (TEM; Hitachi H-7500) has been used to record TEM images of the particles obtained by scratching from the film surfaces and forming a suspension in ethanol solution for TEM grid. The surface morphology has been studied by field emission scanning electron microscope (FE-SEM; HITACH S-4700) operated at 15 kV with 102 pA. Elemental composition has been checked using the energy dispersive X-ray microanalyzer (EMAX; HORIBA-7200H). The surface topography has been studied using atomic force microscope (AFM; NTMDT-NTEGRA) using a silicon nitride cantilever with a stiffness of 0.16 Nm^{-1}. An optical study has been performed using a UV-Vis-NIR double beam spectrophotometer (Perkin-Elmer Lambda-750) in the wavelength range 300 nm-900 nm at room temperature (300 K).

a)Email: pks_phy@yahoo.co.in.

III. RESULTS AND DISCUSSION

The thickness of the deposited CdS nanofilms has been measured to be $t_1 = 39.7$ nm, $t_2 = 65.6$ nm, $t_3 = 87.4$ nm, and $t_4 = 112.5$ nm with an uncertainty of ± 9 nm.

A. XRD analysis

XRD is a non-destructive technique that reveals distinctive diffraction pattern "fingerprint" of crystalline materials used for crystallographic structure, crystallite size, and stress-strain analysis of materials. The XRD spectra of CdS nanofilms as a function of film thickness (Fig. 1) show the existence of multiple reflection peaks signifying the polycrystalline nature of the deposited nanofilms. Besides, the broad profile of XRD peaks indicates nanocrystalline nature due to the presence of nanocrystallites, microstrain, lattice defects, and stacking faults in the films.[15] The diffused background in XRD spectra, predominant in film t_1, may be either due to amorphous glass substrate or due to the presence of amorphous phase in as deposited CdS nanofilms. As the film thickness increases, the interaction between the CdS film and the substrate at the interface becomes less prominent leading to reduction in diffused background of XRD spectra. The structural parameters (Table I) like crystallite size (D_{hkl}), interplanar spacing (d_{hkl}), microstrain (ε_{hkl}), and dislocation density (δ_{hkl}) have been calculated using Debye-Scherrer formula, Bragg's equation, Williamson-Smallman formula, respectively.[11] CdS films deposited by CBD exist in mixed phases (cubic-zinc blende structure, α-CdS and hexagonal-wurtzite structure, β-CdS).[11] All as-deposited nanofilms share mixed α/β-CdS reflections[16] and grow along (*002*) reflection plane parallel to the substrate surface due to its lowest surface free energy[12,17] as shown in Fig. 1. The intensity of the prominent (*002*) reflection peak increases and peak broadening goes on narrowing with increasing thickness. This indicates enhancement of D_{hkl}, reduction of ε_{hkl} and δ_{hkl} in the nanofilms with increasing film thickness (Table I). The peak position of (*002*) reflection shifts toward lower scattering angle (2θ) with increase in film thickness (Table I). The shift, $\Delta(2\theta)$, in the reflection peak position *w.r.t* ideal position of a fault-free sample[16] is related to the stacking fault probability (α_{sf}), given as[18]

$$\alpha_{sf} = \frac{2\pi^2 \Delta(2\theta)}{45\sqrt{3}\tan\theta}. \quad (1)$$

Film t_1 has high ε_{hkl} and δ_{hkl} may lead to build up large stress in the layers. Also films with minimal thickness show higher

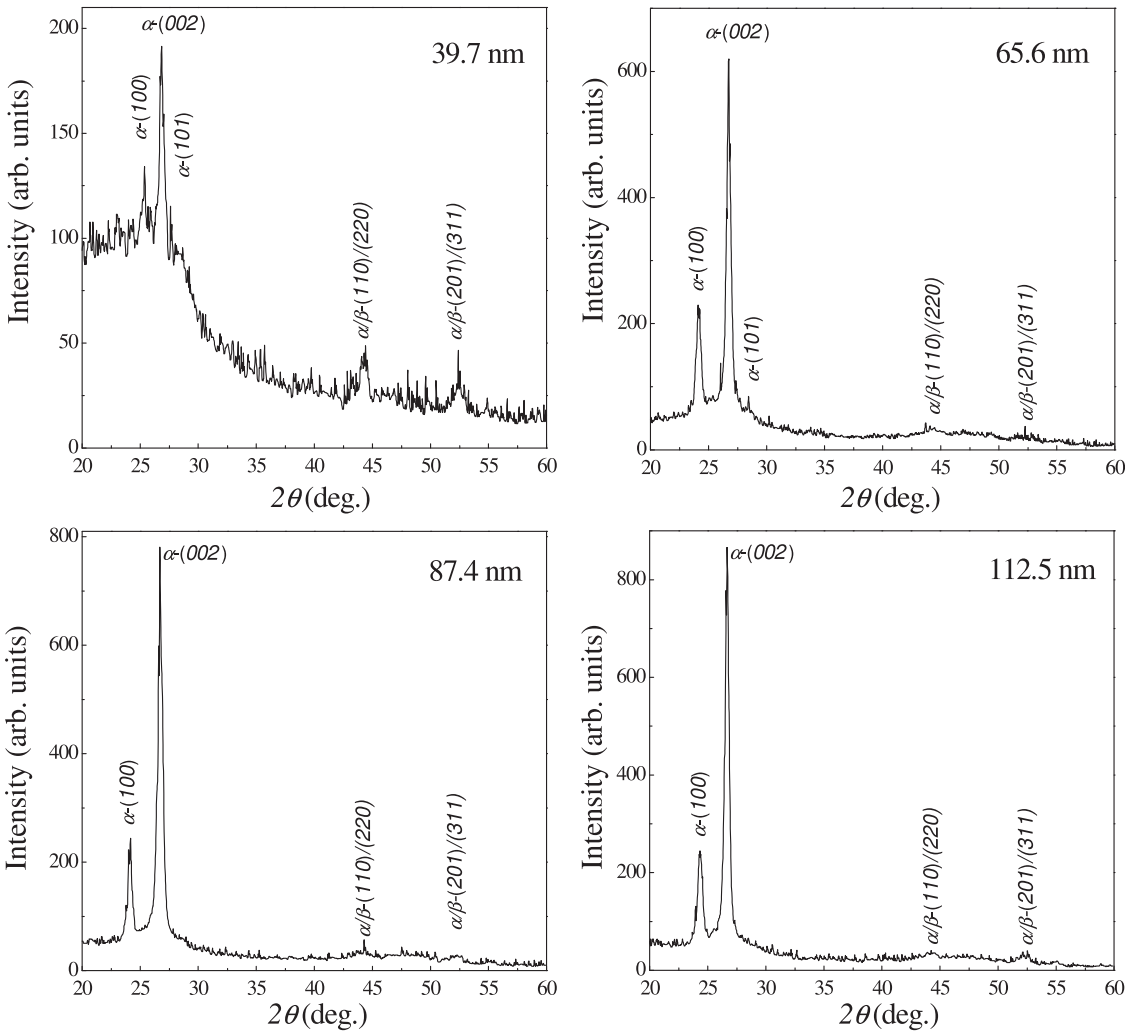

FIG. 1. XRD spectrum for CdS nanofilms with thickness $t_1 = 39.7$ nm, $t_2 = 65.6$ nm, $t_3 = 87.4$ nm, and $t_4 = 112.5$ nm.

TABLE I. The values of crystallite size (D_{hkl}), inter-planar spacing (d_{hkl}), microstrain (ε_{hkl}), dislocation density (δ_{hkl}), stacking fault probability (α_{sf}), lattice constant ratio (c/a), texture coefficient ($TC_{(200)}$), and at. % Cd/S for CdS nanofilms.

Sample	D_{hkl} (nm)	d_{hkl} (Å)	$\varepsilon_{hkl} \times 10^{-3}$	$\delta_{hkl} \times 10^{15}$ line.m^{-2}	a_{sf}	c/a	$TC_{(200)}$	Cd/S
t_1	16.33 ± 0.63	3.318	9.14	3.75	0.066	1.552	2.38	0.93
t_2	17.01 ± 0.71	3.331	8.83	3.46	0.047	1.564	3.59	1.01
t_3	18.56 ± 0.84	3.337	8.09	2.90	0.036	1.571	3.85	1.08
t_4	21.49 ± 1.13	3.340	6.99	2.17	0.031	1.584	4.00	1.10

mismatch between the film surface and the substrate[19] hence exhibits maximum α_{sf} (Table I). As the film thickness increases, the decrease of ε_{hkl} and δ_{hkl} parameters may lead to relaxation of the stress in the films. This indicates that the saturation of crystallite growth on relaxation of the misfit strain between the film and substrate with increase in thickness of the films and hence α_{sf} decreases (Table I). Similar effect of film thickness on the microstrain, dislocation density, and stacking fault probability has been reported.[18,20] The increase in crystallite size with film thickness is a general observation during film growth and has been reported.[21,22] The film thickness affects various physical parameters responsible for the development of crystal structure and, hence, influences the lattice parameters. The lattice constants, $c = 2d_{002}$ and $a = 2d_{100}/\sqrt{3}$, have been obtained (Table I) using values of interplanar spacing of the (*002*) planes (d_{002}) and the (*100*) planes (d_{100}).[17] The c/a ratio for nanofilms is found to be <5% than the ideal value (1.633) for β-CdS structure[16] and approaches towards it with increase in thickness. The low value of c/a ratio and an increase in d_{hkl} imply that the as-deposited nanofilms are under tensile strain along its (*002*) plane parallel to *c*-axis. The film thickness has a direct impact on the texture of the growing material. Conversely, the physical properties of the material as well as the performance and reliability of the fabricated devices is drastically affected by the texture of the material. The texture coefficient (TC_{hkl}) is a measure of the degree of orientation of each reflection in contrast to a randomly oriented sample represented as[23]

$$TC_{(h_ik_il_i)} = \frac{I_{(h_ik_il_i)}}{Io_{(h_ik_il_i)}} \left\{ \frac{1}{N} \sum_{i=1}^{N} \frac{I_{(h_ik_il_i)}}{Io_{(h_ik_il_i)}} \right\}^{-1}, \qquad (2)$$

where $I_{(h_ik_il_i)}$is the diffraction intensity of $(h_ik_il_i)$ plane of the sample under investigation and $Io_{(h_ik_il_i)}$ is the intensity of $(h_ik_il_i)$ plane of the standard sample,[16] and N is the number of reflections present in XRD pattern. The calculated values of $TC_{(hkl)}$ have been listed in Table I. The higher value of $TC_{(200)}$ (>1) indicates that deposited nanofilms have higher degree of orientation along *c*-axis. The value of $TC_{(200)}$ goes on increasing with film thickness indicating improvement of crystallinity and compactness in the film structure. Therefore, the evolution of texture during film growth process has a strong effect on the progress of surface features of the crystallites.

It has been observed that structural parameters like ε_{hkl}, δ_{hkl}, and α_{sf} are inversely related to film thickness. There is reduction in the lattice imperfection and strain with increase in film thickness. However, D_{hkl}, d_{hkl}, c/a, and $TC_{(hkl)}$ are directly related to the film thickness, which indicates that crystallization and orientation of the crystal growth gets enhanced with increase in film thickness.

B. TEM analysis

TEM is a high spatial resolution structural and chemical characterization tool which is capable of imaging crystalline specimen close to interatomic distances. The TEM micrographs for CdS nanofilm (t_2) at two different positions (Fig. 2) and the corresponding selected area diffraction (SAD) pattern

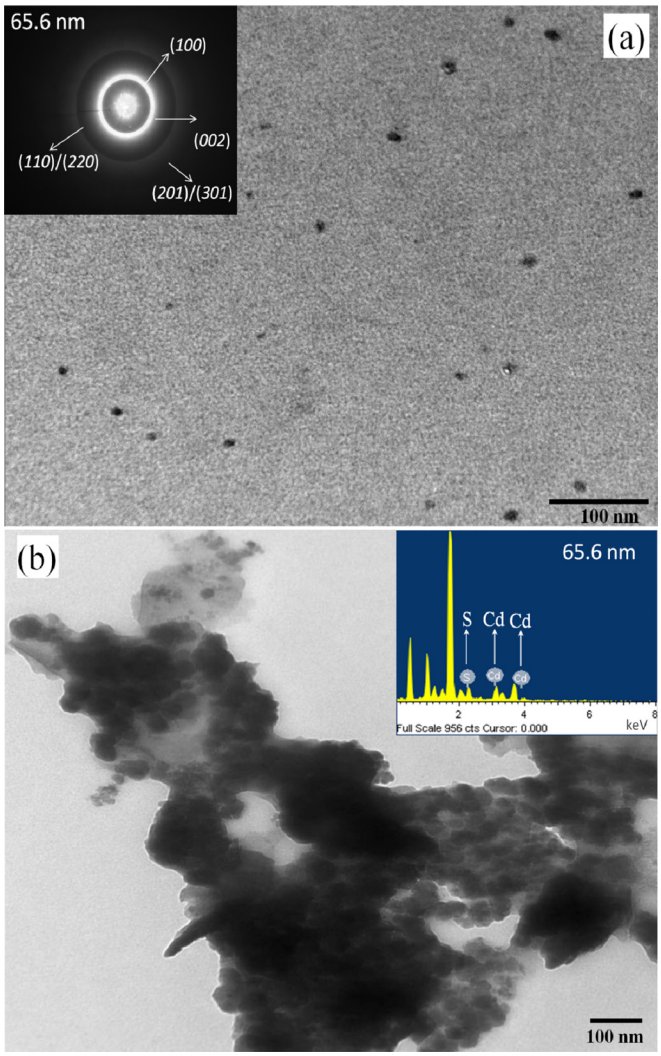

FIG. 2. (a) TEM image at first position for $t_2 = 65.6$ nm. Inset shows SAD pattern. (b) TEM image at second position for t_2 film. Inset shows EDAX spectrum.

(inset of Fig. 2(a)) confirms the polycrystalline nature. There exists a small amount of individually available nanocrystallites and a large amount of small nanocrystallites dispersed fully in the background (Fig. 2(a)). The average size of individually available nanocrystallites has been estimated to be ~15 nm. Besides, TEM micrograph at second position in Fig. 2(b) displays a cluster of agglomerated nanocrystallites, adhering to one another indicating the pattern of particles embedded in the film structure. The average size of crystallites has been estimated from Fig. 2(b) and found to be ~20 nm. These TEM measurements are in good agreement with XRD analysis.

C. EDAX analysis

EDAX or energy dispersive X-ray analysis is used for identifying the elemental composition of the specimen, on an area of interest. The Cd/S ratio for film t_1 is <1, indicating Cd deficiency but Cd content for nanofilms goes on increasing with film thickness (Table II). CdS nanofilm (t_2) has been found to be more stoichiometric among all the nanofilms (inset Fig. 2(b)). This may be attributed to the film growth process which is a combination of nucleation and coarsening of ionic species in the solution. The internal fluctuation in the concentration starts the nucleation of the crystallites. The size of the growing crystallites remains nearly independent to the deposition time and only the concentration of crystallites increase initially. The concentration of S^{2-} ions in the solution is large due to rapid thiourea hydrolysis which decreases with increase in deposition time and decrease in *p*H. As the concentration of precursors drops below a critical concentration, the crystallites start agglomerated quickly with progress in film deposition. Consequently, the concentration of Cd^{2+} ions increases in the solution with time for films with more thickness. Therefore, there is an improvement in crystallite size and increase in agglomeration with a capture of more free Cd^{2+} ions from the solution. The nanofilms (t_2 to t_4) are rich in Cd content with large crystallite size and roughness.

D. FE-SEM analysis

Scanning electron microscopy (SEM) gives an indication of the surface features of film and the crystal growth on the substrate. Fig. 3 shows that the surface morphology of CdS nanofilms depends on the film thickness. All nanofilms have smooth, homogeneous, and uniform surfaces with randomly oriented spherical nanocrystallites. This spherical symmetry may be due to large surface energy of nano crystallites. These nano crystallites show good adhesion to the substrate covering complete surface due to Triton (TX-100).[11,24] The average crystallite size (D_{SEM}) of intermediate particles has been calculated (Table II). CdS nanofilm (t_1) has minimum thickness with least density of packed spherical crystallites indicating lesser agglomeration of nanocrystallites. For CdS nanofilms t_2 and t_3, the agglomeration is prominent. The compactness increases with increase in thickness (see Fig. 3). The crystallites settle in the unoccupied spaces with progress in deposition time resulting in a dense crystalline textured film structure. With the increase in thickness (film t_4), growth of crystallites attains saturation and separates from each other by well defined grain boundaries.

E. AFM analysis

AFM provides two dimensional and three dimensional images of surfaces. Figs. 4(a) and 4(b) shows 2D and 3D AFM images of CdS nanofilms over a scan area of $2 \times 2\ \mu m^2$ recorded in the semi-contact mode. All nanofilms are composed of round shape crystallites. The average crystallite size (D_{AFM}), root mean square roughness (R_{rms}), surface skewness (S_{sk}), and coefficient of kurtosis (S_{ka}) have been obtained by AFM (shown in Table II). The surface grains in the deposited CdS nanofilms have a small D_{AFM} and R_{rms} for t_1 and large for t_4 indicating that D_{AFM} and R_{rms} increase with film thickness enhancing the texture of the film (Fig. 4(a)). This may be due to the agglomeration of crystallites and increase in density Cd^{2+} ions with increase in film thickness (also verified by EDAX). The increase of R_{rms} has also been identified by the bright spots in AFM images (see Fig. 4(a)). There is gradual flattening in the shape of the crystallites, i.e., decrease in S_{sk}, S_{ka} and increase in R_{rms} with the increasing thickness (Fig. 4(b)). The flat peaks with round top and flat faces of the crystallites indicate columnar structural growth corresponding to the hexagonal-wurtzite CdS structure with (*002*) crystalline orientation.[12]

F. Optical analysis

UV-Vis-NIR spectroscopy helps to study optical behaviour and crystallite size of materials. All nanofilms have been observed to be highly transparent with an average optical transparency (*%T*) of >70% and low average reflectance (*%R*) <20% in the visible and NIR region of solar spectrum as shown in Fig. 5. The transmission of the light through the material depends upon the extent of absorption and scattering. There is decrease of *%T* for all films with increase in

TABLE II. The values of crystallite size (D_{SEM} and D_{AFM}), surface roughness (R_{rms}), surface skewness (S_{sk}), coefficient of kurtosis (S_{ka}), absorption coefficient (α), Urbach energy (E_u), sub band gap (E_g^{sub}), optical band gap (E_g), refractive index (n_f), extinction coefficient (k_f), and packing density (p_f) for CdS nanofilms.

Sample	D_{SEM} (nm)	D_{AFM} (nm)	R_{rms} (nm)	S_{sk}	S_{ka}	$\alpha \times 10^4$ (cm^{-1})	E_u	E_g^{sub}	E_g	n_f	k_f	p_f
t_1	15	15.2	5.76	1.39	3.81	5.80	0.623	2.18	2.88	1.71	0.20	0.68
t_2	22	18.5	7.32	1.05	3.01	4.48	0.554	2.20	2.83	1.85	0.21	0.75
t_3	25	19.8	7.86	0.83	2.87	4.12	0.323	2.24	2.67	1.96	0.24	0.79
t_4	35	25.4	8.72	0.70	2.75	3.02	0.282	2.27	2.61	2.06	0.27	0.84

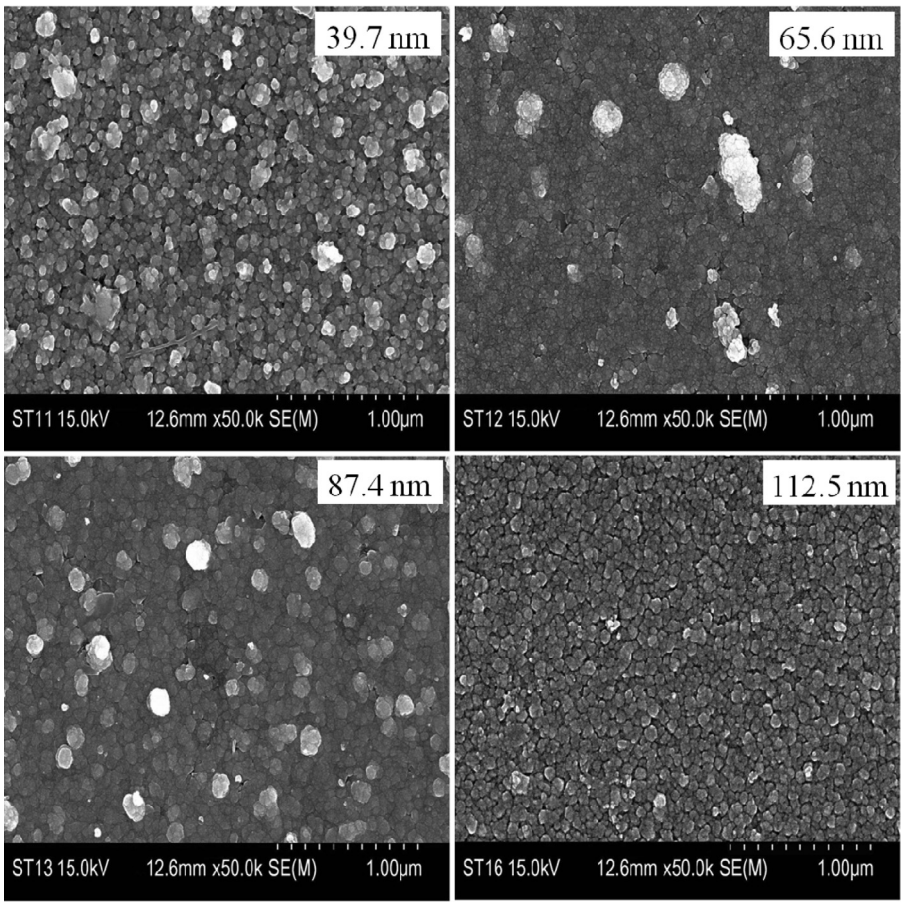

FIG. 3. The FE-SEM micrographs for CdS nanofilms with thickness $t_1 = 39.7$ nm, $t_2 = 65.6$ nm, $t_3 = 87.4$ nm, and $t_4 = 112.5$ nm.

thickness. The relatively low $\%T$ for film t_1 may be due to poor crystallinity and large amorphous component. An increase in film thickness offers a dense structure with improved crystallinity and surface roughness. This is responsible for high absorption and scattering of light leading to decreases in $\%T$ from t_2 to t_4.[4,25] However, the $\%R$ depends on surface roughness and increasing film thickness enhances $\%R$. The extension of $\%T$ observed in low wavelength region up to 300 nm indicates disorders amorphous content in films.[26] This may act as trap centers for radiations affecting the

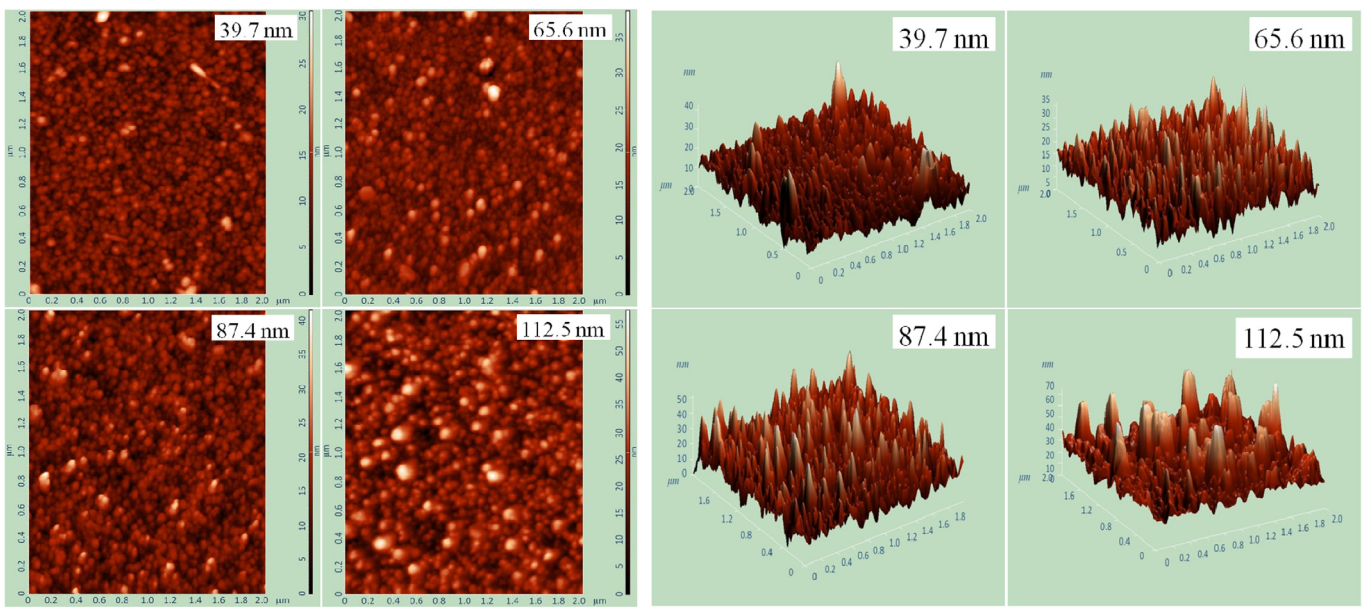

FIG. 4. (a) The 2 dimensional AFM images for CdS nanofilms. (b) The 3 dimensional AFM images for CdS nanofilms with thickness $t_1 = 39.7$ nm, $t_2 = 65.6$ nm, $t_3 = 87.4$ nm, and $t_4 = 112.5$ nm.

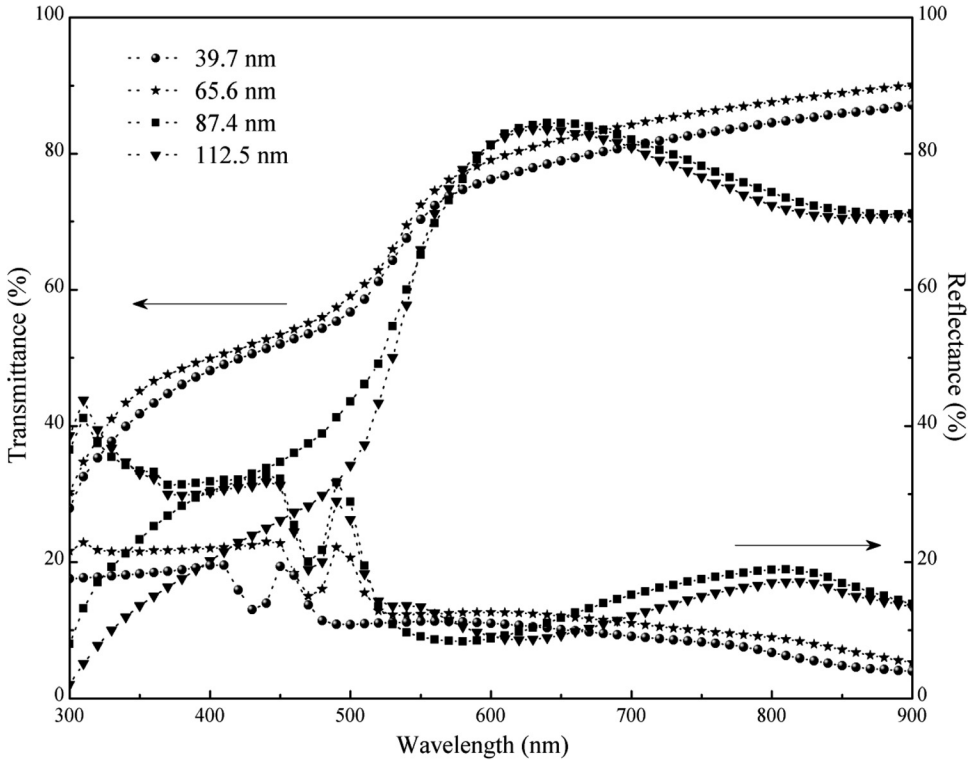

FIG. 5. Transmittance and reflectance spectra for CdS nanofilms with thickness $t_1 = 39.7$ nm, $t_2 = 65.6$ nm, $t_3 = 87.4$ nm, and $t_4 = 112.5$ nm.

absorption. The absorption coefficient (α) signifies inter-band transition near the band gap and has been calculated using[27]

$$\alpha = \frac{1}{t}\ell n, \left[\frac{(1-R)^2}{2T} + \left(\frac{(1-R)^4}{4T^2} + R^2\right)^{1/2}\right], \quad (3)$$

where t, T, and R are film thickness, transmittance, and reflectance, respectively.

The value of α decreases with increase in thickness of the deposited nanofilms in the band to band absorption region as observed elsewhere.[28,29] The relatively high values of α ($\sim 10^5\,\mathrm{cm}^{-1}$) at fundamental absorption edge (Table II) may be due to increase in crystallite size, increase in light absorption/scattering with surface roughness (Fig. 4(b)), and decrease in structural imperfections. In all nanofilms under investigation, a shift in absorption edge towards higher wavelengths with increasing film thickness has been observed (Fig. 5) besides, shows blue shift in comparison to bulk CdS (512 nm).

A rapid rise in α near the fundamental absorption edge indicates direct energy transition in the forbidden gap.[30] For direct allowed transition, Tauc related the absorption coefficient (α) and incident photon energy ($h\nu$) as[4]

$$(\alpha h\nu) = B(h\nu - E_g)^m, \quad (4)$$

where B is characteristic disorder parameter and $m = 1/2$ for direct transition between valance band and conduction band. The optical band gap (E_g) has been estimated (Fig. 5) by extrapolation $(\alpha h\nu)^2 \rightarrow 0$. The value of E_g decreases with increase in thickness (Table II). This may be due to increase in crystallite size, decrease in stacking faults and crystal imperfection (Table I) which results in orientation of the individual crystallites and defect-free grain boundaries. The high value of E_g in the nanofilms in comparison to bulk CdS may be attributed to the quantum confinement associated with the existence of nanocrystallites in the semiconductor material and the low-dimensional film structure. The structural imperfection in the deposited films may be associated with the existence of the onset sub-band gap (E_g^{sub}) along with E_g (Fig. 6).[26,31] From Table II, the increase in E_g^{sub} with thickness may also be explained in terms of Urbach energy (E_u). E_u, the width of tail states in low absorption coefficient region ($<10^4\,\mathrm{cm}^{-1}$), decreases with increase in film thickness. Hence, slope in Fig. 6 increases indicating improvement in ordered crystalline structure with increase in thickness. The decrease of defects states between conduction band and valence band increases the probability of transition.[31] Hence, E_g and E_u decrease whereas E_g^{sub} increases with increase in film thickness.

The optical constants (refractive index (n_f) and extinction coefficient (k_f)) explain the interaction of light travelling through the materials and their value changes with frequency of light. These constants play an important role in deciding optoelectronic properties of the material. The values of n_f and k_f have been calculated (Table II).[27] The Cauchy fitting[32] has been employed to study the normal dispersion behaviour of both n_f and k_f in the wavelength range of 300 nm-900 nm (Fig. 7). The refractive indices show normal dispersion behaviour with wavelength for all nanofilms due to polarization in material with wavelength. The value of n_f increases with thickness of the films (Table II). This may be attributed to increase in crystallite size (film thickness) with the relaxation of microstrain with thickness. The extinction coefficient is directly influenced by the corresponding absorption coefficient and influenced by

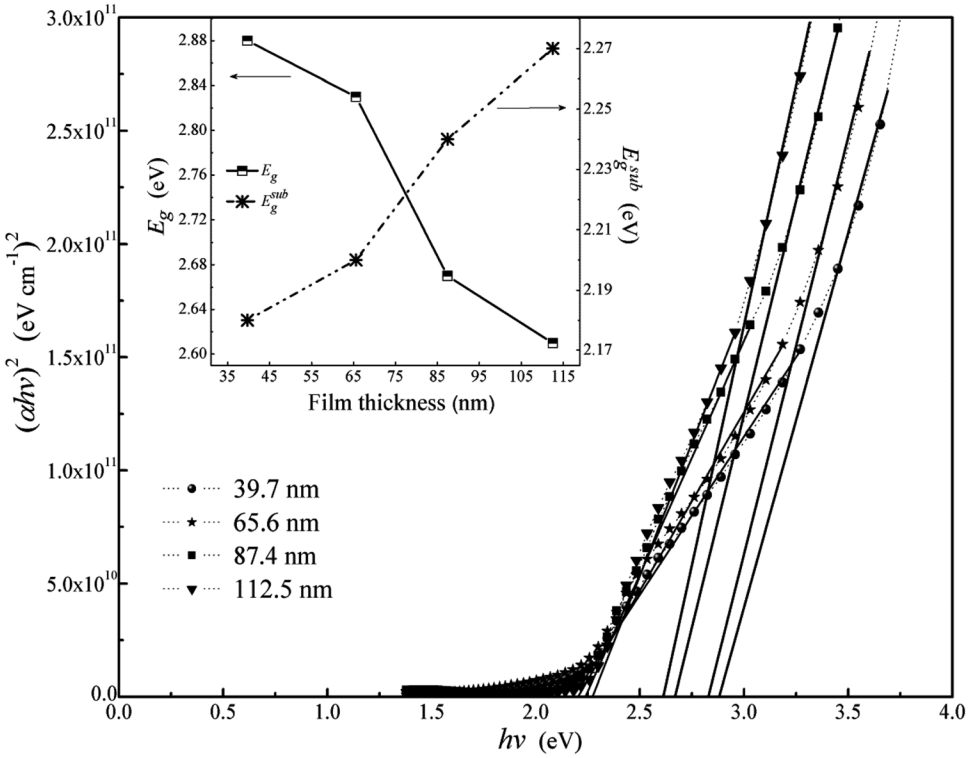

FIG. 6. Plot of $(\alpha h\nu)^2$ versus $h\nu$. Inset shows the variation of E_g and E_g^{sub} as a function of film thickness.

film thickness. The dispersion of k_f with wavelength has been shown in the inset of Fig. 7 while values of k_f calculated from saturation point are in Table II. The increase in the value of n_f and k_f with thickness indicates that the light traveling through CdS nanofilms experiences attenuation due to loss of energy. This may be account for various loss mechanisms *viz.* generation of phonons (lattice waves), photo-generation, free carrier absorption, scattering, crystallite size, and denser layer structure with increase in thickness.[33,34] As the wavelength increases in visible range, dispersion decreases for both n_f and k_f (13.6% and 27.0% for t_1, 15.9% and 28.3% for t_2, 26.6% and 33.3% for t_3, 23.9% and 28.9% for t_4).

This increase of refractive index with film thickness may also be understood on the basis of packing of crystallites in the film structure. The increase in film thickness is able to reduce the voids and thin areas in the film structure. The

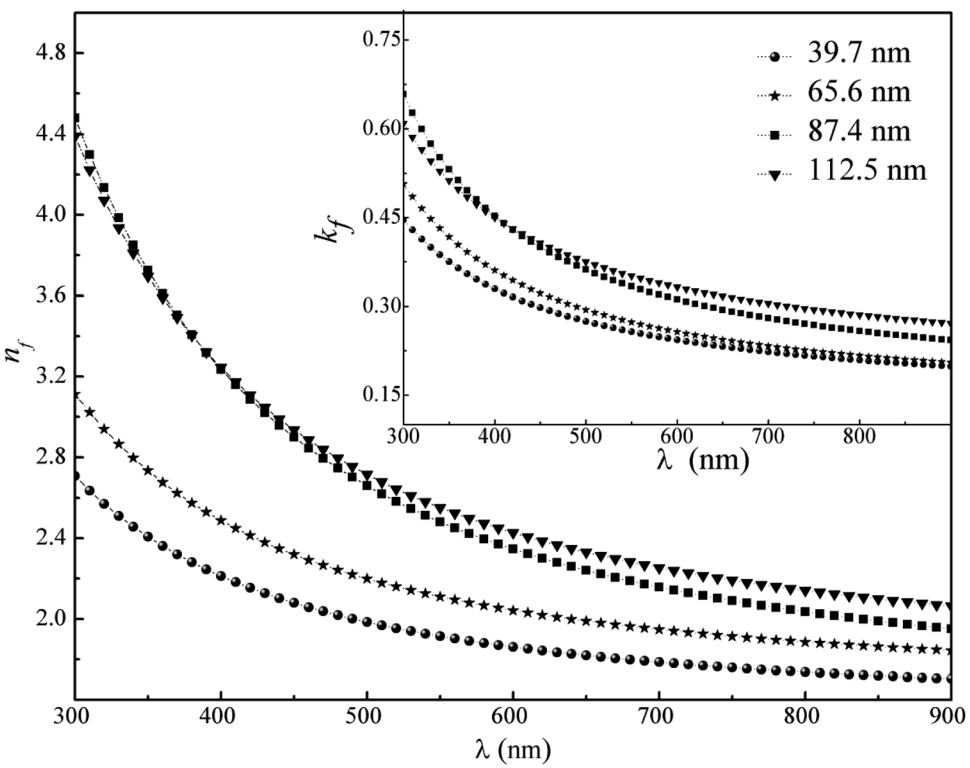

FIG. 7. Plot of n_f versus λ. Inset shows the plot of k_f versus λ for CdS nanofilms with thickness $t_1 = 39.7$ nm, $t_2 = 65.6$ nm, $t_3 = 87.4$ nm, and $t_4 = 112.5$ nm.

packing density (p_f) and lattice parameter (c_f) are related to each other and may change the value of n_f according to relation,[35]

$$n_f = \sqrt{\frac{(1-p_f)n_v^4 + (1+p_f)n_v^2 n_b^2}{(1+p_f)n_v^2 + (1-p_f)n_b^2}} + \frac{5}{2}\left(\frac{n_b^2 - 1}{n_b c_b}\right)(c_f - c_b), \tag{5}$$

where n_f, n_b, and n_v are refractive indices for film, bulk crystal, and void, respectively. c_b is bulk lattice parameter. The values of p_f (Table II) show that the density of packing of crystallites in the films increase with thickness leads to increasing n_f.

The complex dielectric constant (ε^*) is a fundamental material property which is closely related to optical constants. The real part of the dielectric constant (ε_r) signifies the dispersion while the imaginary part (ε_i) relates to the dissipation of the light in the material. Both ε_r and ε_i are represented by relation $\varepsilon^* = \varepsilon_r + \varepsilon_i = (n_f - ik_f)^2$.[34] The values of $\varepsilon_r/\varepsilon_i$ are found to 2.88/0.68, 3.38/0.78, 3.78/0.94, and 4.17/1.11 for t_1 to t_4, respectively. The factor $\varepsilon_i/\varepsilon_r$ measures the inherent dissipation of electromagnetic energy of a dielectric material which increases with thickness. The optical conductivity (σ) describes the dissipation of e.m. energy in the material and proportional to absorption energy as

$$\sigma = \frac{\alpha n_f c}{4\pi}, \tag{6}$$

where c is the velocity of light. The values of σ are found to be $2.37 \times 10^{14}\ \Omega^{-1}\mathrm{m}^{-1}$, $1.98 \times 10^{14}\ \Omega^{-1}\mathrm{m}^{-1}$, $1.93 \times 10^{14}\ \Omega^{-1}\mathrm{m}^{-1}$, and $1.49 \times 10^{14}\ \Omega^{-1}\mathrm{m}^{-1}$ for t_1 to t_4, respectively. σ is maximum for t_1 exhibiting high α and low n_f while minimum for t_4 with low α and high n_f. The overall high values of σ for all nanofilms increase the photo response behaviour and make them suitable for optoelectronic applications.

IV. CONCLUSION

The XRD study shows polycrystalline films with prominent wurtzite structure having (*002*) orientation. The crystallite size and surface roughness of the nanofilms increases with film thickness. With increase in film thickness, the lattice parameter increases relaxing the inherent strain and dislocations. The absorption edge of nanofilms lies in lower wavelength region in comparison to bulk CdS indicating quantum effect. Optical band gap and Urbach energy decrease with an increase in film thickness. The refractive index and extinction coefficient show normal dispersion and increase with an increase in film thickness. These properties make CdS nanofilms suitable for optoelectronic, photovoltaic and visible light detection application.

ACKNOWLEDGMENTS

The authors acknowledge H.P University Shimla, SAIF P.U. Chandigarh, and IIT Roorkee for providing XRD, TEM, and AFM facilities, respectively.

[1]H. Murai, T. Abe, J. Matsuda, H. Sato, S. Chiba, and Y. Kashiwaba, Appl. Surf. Sci. **244**, 351 (2005).
[2]A. Romeo, D. L. Batzner, H. Zogg, C. Vignali, and A. N. Tiwari, Sol. Energy Mater. Sol. Cells **67**, 311 (2001).
[3]R. M. Perez, J. S. Hernandez, G. C. Puente, and O. V. Galan, Sol. Energy Mater. Sol. Cells **93**, 79 (2009).
[4]S. Kumar, P. Sharma, and V. Sharma, J. Appl. Phys. **111**, 043519 (2012).
[5]J. Zhao, J. A. Bardecker, A. M. Munro, M. S. Liu, Y. Niu, I. K. Ding, J. Luo, B. Chen, A. K. Y. Jen, and D. S. Ginger, Nano Lett. **6**, 463 (2006).
[6]S. G. Hur, E. T. Kim, J. H. Lee, G. H. Kim, and S. G. Yoon, J. Vac. Sci. Technol. B **26**, 1334 (2008).
[7]P. Liu, V. P. Singh, C. A. Jarro, and S. Rajaputra, Nanotechnology **22**, 145304 (2011).
[8]P. O'Brien and J. McAleese, J. Mater. Chem. **8**, 2309 (1998).
[9]G. Hodes, Phys. Chem. Chem. Phys. **9**, 2181 (2007).
[10]H. Khallaf, I. O. Oladeji, G. Cha, and L. Chow, Thin Solid Films **516**, 7306 (2008).
[11]S. Kumar, P. Sharma, and V. Sharma, J. Appl. Phys. **111**, 113510 (2012).
[12]C. D. G. Lazos, E. Rosendo, B. H. Juarez, G. G. Salgado, T. Diaz, M. R. Falfan, A. I. Oliva, P. Quintana, D. H. Aguilar, W. Cauich, M. Ortega, and Y. Matsumoto, J. Electrochem. Soc. **155**, D158 (2008).
[13]J. P. Enriquez and X. Mathew, Sol. Energy Mater. Sol. Cells **76**, 313 (2003).
[14]N. S. Das, P. K. Ghosh, M. K. Mitra, and K. K. Chattopadhyay, Physica E **42**, 2097 (2010).
[15]S. N. Dey, P. Chatterjee, and S. P. S. Gupta, J. Appl. Phys. **100**, 073509 (2006).
[16]JCPDS-data file Nos. 06-0314 and 89-0440.
[17]A. E. Rakhshani and A. S. Al-Azab, J. Phys.: Condens. Matter **12**, 8745 (2000).
[18]U. Pal, D. Samanta, S. Ghorai, B. K. Samantaray, and A. K. Chaudhuri, J. Phys. D: Appl. Phys. **25**, 1488 (1992).
[19]J. Cao and J. Wua, Mat. Sci. Eng. R **71**, 35 (2011).
[20]H. L. Chen, Y. M. Lu, and W. S. Hwang, JIM Mater. Trans. **46**, 872 (2005).
[21]H. Kim, J. S. Horwitz, G. Kushto, A. Pique, Z. H. Kafafi, C. M. Gilmore, and D. B. Chrisey, J. Appl. Phys. **88**, 6021 (2000).
[22]S. Lalitha, R. Sathyamoorthy, S. Senthilarasu, A. Subbarayan, and K. Natarajan, Sol. Energy Mater. Sol. Cells **82**, 187 (2004).
[23]J. Gao, W. Jie, Y. Yuan, T. Wang, G. Zha, and J. Tong, J. Vac. Sci. Technol. A **29**, 051507 (2011).
[24]C. L. Perkins and F. S. Hasoon, J. Vac. Sci. Technol. A **24**, 497 (2006).
[25]J. H. Lee, W. C. Song, J. S. Yi, K. J. Yang, W. D. Han, and J. Hwang, Thin Solid Films **431–432**, 349 (2003).
[26]F. Liu, Y. Lai, J. Liu, B. Wang, S. Kuang, Z. Zhang, J. Li, and Y. Liu, J. Alloys Compd. **493**, 305 (2010).
[27]A. M. Salem, Y. A. El-Gendy, G. B. Sakr, and W. Z. Soliman, J. Phys. D: Appl. Phys. **41**, 025311 (2008).
[28]H. Metin and R. Esen, Semicond. Sci. Technol. **18**, 647 (2003).
[29]E. Cetinorgu, C. Gumus, and R. Esen, Thin Solid Films **515**, 1688 (2006).
[30]M. C. Jun and J. H. Koh, Nanoscale Res. Lett. **7**, 294 (2012).
[31]A. Meeder, D. F. Marron, A. Rumberg, M. C. Lux-Steiner, V. Chu, and J. P. Conde, J. Appl. Phys. **92**, 3016 (2002).
[32]Z. H. Dai, R. J. Zhang, J. Shao, Y. M. Chen, Y. X. Zheng, J. D. Wu, and L. Y. Chen, J. Korean Phys. Soc. **55**, 1227 (2009).
[33]H. Adamska and H. N. Spector, J. Appl. Phys. **56**, 1123 (1984).
[34]W. C. Tan, K. Koughia, J. Singh, and S. O. Kasap, "Fundamental optical properties of materials I," in *Optical Properties of Condensed Matter and Applications*, edited by J. Singh (John Wiley & Sons, Chichester, 2006), Chap. 1.
[35]H. K. Yadav, K. Sreenivas, and V. Gupta, J. Appl. Phys. **99**, 083507 (2006).